NASA/TM-2003-212665

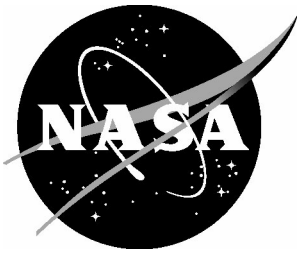

A Flight Dynamics Model for a Small Glider in Ambient Winds

Scott C. Beeler
National Institute of Aerospace, Hampton, Virginia

Daniel D. Moerder and David E. Cox
Langley Research Center, Hampton, Virginia

November 2003

The NASA STI Program Office . . . in Profile

Since its founding, NASA has been dedicated to the advancement of aeronautics and space science. The NASA Scientific and Technical Information (STI) Program Office plays a key part in helping NASA maintain this important role.

The NASA STI Program Office is operated by Langley Research Center, the lead center for NASA's scientific and technical information. The NASA STI Program Office provides access to the NASA STI Database, the largest collection of aeronautical and space science STI in the world. The Program Office is also NASA's institutional mechanism for disseminating the results of its research and development activities. These results are published by NASA in the NASA STI Report Series, which includes the following report types:

- TECHNICAL PUBLICATION. Reports of completed research or a major significant phase of research that present the results of NASA programs and include extensive data or theoretical analysis. Includes compilations of significant scientific and technical data and information deemed to be of continuing reference value. NASA counterpart of peer-reviewed formal professional papers, but having less stringent limitations on manuscript length and extent of graphic presentations.

- TECHNICAL MEMORANDUM. Scientific and technical findings that are preliminary or of specialized interest, e.g., quick release reports, working papers, and bibliographies that contain minimal annotation. Does not contain extensive analysis.

- CONTRACTOR REPORT. Scientific and technical findings by NASA-sponsored contractors and grantees.

- CONFERENCE PUBLICATION. Collected papers from scientific and technical conferences, symposia, seminars, or other meetings sponsored or co-sponsored by NASA.

- SPECIAL PUBLICATION. Scientific, technical, or historical information from NASA programs, projects, and missions, often concerned with subjects having substantial public interest.

- TECHNICAL TRANSLATION. English-language translations of foreign scientific and technical material pertinent to NASA's mission.

Specialized services that complement the STI Program Office's diverse offerings include creating custom thesauri, building customized databases, organizing and publishing research results ... even providing videos.

For more information about the NASA STI Program Office, see the following:

- Access the NASA STI Program Home Page at ***http://www.sti.nasa.gov***

- E-mail your question via the Internet to help@sti.nasa.gov

- Fax your question to the NASA STI Help Desk at (301) 621-0134

- Phone the NASA STI Help Desk at (301) 621-0390

- Write to:
  NASA STI Help Desk
  NASA Center for AeroSpace Information
  7121 Standard Drive
  Hanover, MD 21076-1320

NASA/TM-2003-212665

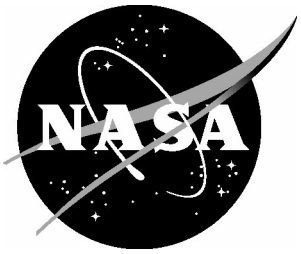

A Flight Dynamics Model for a Small Glider in Ambient Winds

Scott C. Beeler
National Institute of Aerospace, Hampton, Virginia

Daniel D. Moerder and David E. Cox
Langley Research Center, Hampton, Virginia

National Aeronautics and
Space Administration

Langley Research Center
Hampton, Virginia 23681-2199

November 2003

Acknowledgments

The authors would like to thank Peter Lissaman for his helpful comments on an earlier draft of this paper.

Abstract. In this paper we describe the equations of motion developed for a point-mass zero-thrust (gliding) aircraft model operating in an environment of spatially varying atmospheric winds. The wind effects are included as an integral part of the flight dynamics equations, and the model is controlled through the three aerodynamic control angles. Formulas for the aerodynamic coefficients for this model are constructed to include the effects of several different aspects contributing to the aerodynamic performance of the vehicle. Characteristic parameter values of the model are compared with those found in a different set of small glider simulations. We execute a set of example problems which solve the glider dynamics equations to find the aircraft trajectory given specified control inputs. The ambient wind conditions and glider characteristics are varied to compare the simulation results under these different circumstances.

Section 1: Introduction

Small unpiloted aircraft (UAVs) are conceptually attractive for surveillance, communication relay, and other loitering-dominated missions. This is because the lack of an on-board pilot eliminates risk to human life, and because vehicle cost tends to shrink with the size of the vehicle. In the missions considered for such aircraft, a substantial capacity for loitering endurance is needed and, indeed, it can be asserted that there is no practical upper limit in the amount of loiter capacity that is desirable.

Small UAVs currently contemplated or deployed typically use propulsion to provide energy to the airframe. This requires fuel to be carried (placing a ceiling on endurance and driving system mass up) or requires that the vehicle carries a "sufficiently large" array of solar cells and batteries to stay aloft. Difficulties with these options motivate exploration of alternate paths to mission endurance.

One of these is to extract energy from the ambient atmospheric velocity field through which the aircraft flies, as is done naturally by large soaring birds – consider, for example, vultures thermalling over carrion. This option is attractive because, superficially, the energy is "free" – assuming that the aircraft is configured to soar well (like a sailplane), it need only fly in a certain way and it will gather sufficient energy from ambient atmospheric motion to stay aloft.

The complication encountered here is that the aircraft's flight path must simultaneously satisfy mission performance requirements and atmospheric energy extraction requirements. A simulation model of such a vehicle is needed in order to carry out the analyses leading to such mission designs, and one is provided in this paper, for the case of purely gliding flight. The key features of the model provided are as follows:

- The airframe dynamics are represented in point mass form, fully accounting for the three-dimensional velocity of the atmosphere, an arbitrary function of location in an Earth-fixed coordinate system. The atmosphere representation can be time-dependent, if desired, but since the equations of motion are autonomous, such time dependence will not appear explicitly.

- A parametric model for aerodynamic lift, drag, and side force coefficients is constructed, based on a similar model of very small aircraft [1]. The model is parameterized on vehicle wingspan (between 60 and 140 inches) and aspect ratio (between 6 and 16). The weight of the vehicle is also used as a variable parameter in the overall glider model.

These features differentiate the above model from those typically provided for powered flight of full-sized vehicles. In the latter case, the vehicle's velocity is typically overwhelmingly larger than that of the atmospheric wind through which it flies; winds, in this case, can be either ignored or treated as small disturbances. For small gliders, on the other hand, the norm of the ambient wind may quite possibly exceed that of the vehicle's velocity. Similarly, it is important that the model reflect the aerodynamics of small, slow, vehicles given that drag in particular is a strong function of Reynolds number.

The glider model will be described in the next three sections of the paper, beginning with the basic equations of motion in Section 2. The basic aerodynamic force equations (without wind) are then described in Section 3, followed by the addition of wind influence and construction of the full model in Section 4. In Section 5 the method of finding values for the aerodynamic force coefficients is described and some resulting characteristic parameters are compared with a literature source. The behavior of the glider model is demonstrated in Section 6 with a set of example problem results looking at solutions of the flight dynamics equations with fixed control inputs. Section 7 gives some overall conclusions about the work described in this paper. Appendix I contains more complete details of the glider model.

Section 2: Glider Equations of Motion

The standard form equations of motion for this point-mass zero-thrust aircraft, given a flat Earth assumption, are [2]:

$$\dot{h} = V \sin\gamma \tag{1}$$

$$\dot{x} = V \cos\chi \cos\gamma \tag{2}$$

$$\dot{y} = V \sin\chi \cos\gamma \tag{3}$$

$$\dot{V} = -\frac{D}{m} - g \sin\gamma \tag{4}$$

$$\dot{\gamma} = \frac{1}{mV}(L\cos\sigma + C\sin\sigma) - \frac{g}{V}\cos\gamma \tag{5}$$

$$\dot{\chi} = \frac{1}{mV\cos\gamma}(L\sin\sigma - C\cos\sigma). \tag{6}$$

These equations define the inertial motion of the aircraft, with g being gravitational acceleration, m the vehicle mass (a known glider characteristic), $V = \|\vec{V}\|$ the vehicle speed, and D, C and L the aerodynamic force components (functions of the glider speed and angles as will be discussed below).

Equations (1-3) give the inertial position rates in an Earth-based coordinate system, also representing components of the velocity $\vec{V} = [\dot{x} \;\; \dot{y} \;\; \dot{z}]^T$ in the directions of the axes in the unit vector set

$$\hat{U}_I \equiv \left[\begin{array}{c|c|c} \hat{x} & \hat{y} & \hat{z} \end{array}\right] = \left[\begin{array}{c|c|c} 1 & 0 & 0 \\ 0 & 1 & 0 \\ 0 & 0 & 1 \end{array}\right] \tag{7}$$

(north, east, and downward respectively), with the modification that instead of the downward z component, equation (1) represents the change in the altitude $h = -z$. Equations (4-6) define the vehicle dynamics, specifying the rates of change of the glider speed and direction. The

azimuth angle χ and elevation angle γ, along with the bank angle σ (a control rotation about the velocity vector $\vec{V}$), form the euler sequence $\{\chi, \gamma, \sigma\}$. This moves from the inertial frame axes to the right-handed set of "velocity frame" axes $\hat{U}_V \equiv [\hat{x}_v \quad \hat{y}_v \quad \hat{z}_v]$, which are aligned with the inertial velocity vector so that $\hat{x}_v = \vec{V}/\|\vec{V}\|$. This rotation is represented by:

$$\hat{U}_V = R_{VI}(\chi, \gamma, \sigma)\hat{U}_I = R_{VI} \tag{8}$$

(since we are in inertial coordinates and so as noted above $\hat{U}_I = I$). Details of this rotation as well as the rest of the equations of motion formulation are given in Appendix I.

Section 3: Aerodynamic Forces With No Wind

The drag, side, and lift forces D, C, and L make up the separate velocity frame components of the overall aerodynamic force vector $F_{A_V} = -D\hat{x}_v - C\hat{y}_v - L\hat{z}_v$. Control of the vehicle model takes place through modulation of the aerodynamic force vector and by rotation of the C and L components via the bank angle σ in equations (5-6). D, C, and L are functions of the aerodynamic angles α (angle of attack) and β (sideslip angle), as well as the glider speed V and a few aircraft and atmospheric parameters.

Along with σ, the angles α and β assume the role of control variables, by changing the direction from which the airmass impacts the vehicle body. The sequence of angles $\{-\beta, \alpha, 0\}$ is used to rotate (about the velocity axes) from the velocity frame axes to the vehicle "body frame" axes $\hat{U}_B \equiv [\hat{x}_b \quad \hat{y}_b \quad \hat{z}_b]$. This rotation is represented by:

$$\hat{U}_B = \left(T_{IV} R_{BV}(-\beta, \alpha, 0) T_{IV}^{-1}\right) \hat{U}_V. \tag{9}$$

Note that the β rotation is negative; this is a convention which we will follow in order to preserve consistency with the flight dynamics literature [2]. The coordinate transformation matrix T_{IV} (which changes a vector from velocity coordinates to inertial coordinates) and its inverse in equation (9) are necessary since the $-\beta$ and α rotations are performed about the velocity axes but we begin and end in inertial coordinates. The transformation matrix is in fact given by $T_{IV} = \hat{U}_V = R_{VI}$, so that equation (9) is rewritten as

$$\hat{U}_B = \left(R_{VI} R_{BV} R_{VI}^{-1}\right) \hat{U}_V. \tag{10}$$

In the absence of wind, the drag, side, and lift forces in the velocity frame are given directly by the chosen formulas

$$D = \bar{q} S C_D(\alpha, \beta) \tag{11}$$

$$C = \bar{q} S C_C(\beta) \tag{12}$$

$$L = \bar{q} S C_L(\alpha), \tag{13}$$

where S is the glider wing surface area, and the dynamic pressure $\bar{q}$ is given by

$$\bar{q} = \frac{1}{2}\rho V^2, \tag{14}$$

with atmospheric density ρ. These force values then can be used in the system (1-6) to express the glider flight dynamics in zero-wind conditions.

The aerodynamic coefficients C_D, C_C, and C_L are functions of the aerodynamic angles in a manner to be discussed in Section 5. This formulation includes more detail than previous models of glider flight in wind [3, 4, 5] which use the coefficient C_L (and C_D as a function of it) directly, rather than as a function of the aerodynamic angles. This extension to angle of attack and sideslip angle dependence will create additional complexity in the present model when wind becomes involved, as will be seen in the next section.

Section 4: Aerodynamic Forces With Ambient Wind

The presence of ambient wind changes our physical interpretation of α and β. They remain control variables with σ, but rather than defining the incidence of the body axes to the incoming airmass, they now only describe the attitude of the body with respect to $\vec{V}$, and will be labeled the "velocity-relative" control angles. The definition of the actual attack, side, and bank angles is in reference to the incoming airflow direction, and so with the addition of ambient wind altering the direction from which the air impacts the vehicle, their meaning will diverge from the velocity-frame-based definition in the last section. We introduce a "wind-relative" reference frame to serve as the midway point in a transformation from inertial to body coordinates that includes the wind effects. Wind-relative force components D_w, C_w and L_w must be computed using newly-found wind-relative angles, before the results are transformed back to velocity coordinates for use in the equations of motion.

Denoting the ambient wind vector as $\vec{w}(h, x, y)$, the wind-relative glider velocity (velocity with respect to the moving airmass) is $\vec{V}_w = \vec{V} - \vec{w}$. We will need to find an euler rotation sequence $\{\chi_w, \gamma_w, \sigma_w\}$ which takes the inertial frame axes to the wind-relative frame axes $\hat{U}_W \equiv [\hat{x}_w \;\; \hat{y}_w \;\; \hat{z}_w]$ (with $\hat{x}_w$ equal to $\vec{V}_w / \|\vec{V}_w\|$), as well as a sequence $\{-\beta_w, \alpha_w, 0\}$ in the wind-relative frame which takes the wind-relative axes to the vehicle body axes. Equation (14) will use the wind-relative speed $V_w = \|\vec{V}_w\|$ instead of V, and equations (11-13) will use α_w and β_w to find D_w, C_w and L_w. These rotational sequences, parallels to equations (8) and (10), are written as:

$$\hat{U}_W = R_{WI}(\chi_w, \gamma_w, \sigma_w)\hat{U}_I, \tag{15}$$

$$\hat{U}_B = \left(R_{WI}R_{BW}(-\beta_w, \alpha_w, 0)R_{WI}^{-1}\right)\hat{U}_W. \tag{16}$$

The angles χ_w and γ_w are found by ensuring that $\hat{x}_w = R_{WI}\hat{x}$. The other wind-relative angles (σ_w, α_w and β_w) must be found by comparing the transitions to the body frame via the velocity frame and the wind-relative frame, so that:

$$\left(R_{WI}R_{BW}R_{WI}^{-1}\right)R_{WI} = \left(R_{VI}R_{BV}R_{VI}^{-1}\right)R_{VI}, \tag{17}$$

which reduces to

$$R_{WI}R_{BW} = R_{VI}R_{BV}. \tag{18}$$

Details of the solution for the angles are given in Appendix I.

The drag, side, and lift forces are calculated starting with equations (11-13), now in terms of the wind-relative angles α_w and β_w, as:

$$D_w = \bar{q}SC_D(\alpha_w, \beta_w) \tag{19}$$

$$C_w = \bar{q}SC_C(\beta_w) \tag{20}$$

$$L_w = \bar{q}SC_L(\alpha_w). \tag{21}$$

The dynamic pressure $\bar{q}$ is given as a function of the wind-relative speed by

$$\bar{q} = \frac{1}{2}\rho V_w^2. \tag{22}$$

However, we want the forces in terms of component values along the velocity axes ($F_{A_V} = [-D \quad -C \quad -L]^T$). Therefore we apply a transformation from $F_{A_W} = [-D_w \quad -C_w \quad -L_w]^T$, in wind-relative coordinates, through inertial coordinates to the final form of the forces:

$$F_{A_V} = R_{VI}^{-1} R_{WI} F_{A_W}. \tag{23}$$

These velocity frame force components are substituted into equations (4-6), along with the original velocity-relative bank angle σ, to control the vehicle dynamics.

Section 5: Aerodynamic Force Coefficient Estimation

The aerodynamic coefficient model is similar to that of the simulation-based soaring performance study of R/C (radio-controlled) model sailplanes by Beron-Rawdon [1]. The model here uses values of parameters from Beron-Rawdon's paper, and the following formulas for the construction of aerodynamic coefficients include most of the constitutive elements of that model as well, although the two are not identical. The representation of aerodynamic effects contributing to the following formulas can be found in sources such as Etkin [2], Perkins and Hage [6], and Anderson [7]. Airfoil performance data is taken from a low Reynolds number airfoil study by Selig et al [8] on which Beron-Rawdon's models were also based. The drag, lift, and side forces will be functions of the angle of attack and side angle of the aircraft (α and β, or when including wind, α_w and β_w), and certain design parameters.

The main design parameters are wingspan ℓ (in), aspect ratio AR, and weight W (lb), which can be varied to test differently structured gliders. Beron-Rawdon uses ranges of ℓ from 60 to 140 in, AR from 6 to 20, and W from roughly 0.5 to 12 lb. The following values are also chosen for simulated small gliders:

- fuselage area S_F (in^2) (a range of values as a function of wingspan, specifically 86, 145, 216, 300, and 396 in^2 for wingspan values of 60, 80, 100, 120, and 140 in^2 respectively),
- fuselage moment arm length (from vehicle center of gravity to both horizontal and vertical tail aerodynamic centers) $\ell_t = 0.28\ell$ (in),
- horizontal tail volume ratio $V_H = 0.4$, vertical tail volume ratio $V_V = 0.02$,
- mean aerodynamic chord $\bar{c} = 1.03\ell/AR$ (in),
- Oswald efficiency factor $e = 0.95$,
- "infinite-span wing" airfoil aerodynamic characteristics from the SD7037 airfoil [8], which for Reynolds number 150,000 has values of lift curve slope $a_0 = 0.1(180/\pi)$ (1/rad), zero point $\alpha_0 = -2.5(\pi/180)$ rad, and wing profile drag given by $C_d = C_{d_0} + C_{d_L}(C_L - C_{L_{min}})^2 = 0.01 + 0.05(C_L - 0.4)^2$,
- fuselage drag coefficient $C_{D_F} = 0.008$, tail drag coefficient $C_{D_T} = 0.01$, and miscellaneous "extra drag" coefficient $C_{D_E} = 0.002$.

Initial calculations find the area values for the various surfaces from the given parameters. The wing surface area is $S = \ell^2/AR$ (in^2), the horizontal tail surface area is $S_T = V_H \bar{c} S/\ell_t$ (in^2), and the vertical tail surface area is $S_V = V_V \ell S/\ell_t$ (in^2).

From the "infinite-span wing" airfoil lift slope value a_0, the finite wing slope is

$$C_{L_\alpha} = \frac{a_0}{1 + a_0/(\pi e AR)} \tag{24}$$

(in units of 1/rad). The angle of attack value where the finite wing lift coefficient $C_L(\alpha) = 0$ is the same value as for the infinite-span wing, α_0. Thus the glider lift coefficient is given by the following function of α:

$$C_L(\alpha) = C_{L_\alpha}(\alpha - \alpha_0). \tag{25}$$

The drag coefficient $C_D(\alpha)$ is built up of several elements. In the vertical plane (ignoring side angle effects for now), these are as follows:

- constant-valued fuselage, tail, and "extra" profile drag values given by $C_{D_F} S_F/S$, $C_{D_T}(S_T + S_V)/S$, and C_{D_E} (the multiplications by surface area ratios are due to the fuselage and tail drag effects acting on those smaller surfaces, not the wing area, and so the use of the ratios will effectively replace the wing area in equations (11-13) by the fuselage and tail areas for the relevant terms),
- wing profile drag $C_d = C_{d_0} + C_{d_L}(C_L - C_{L_{min}})^2$, from the airfoil data,
- induced drag from lift of $C_{D_\alpha} = C_L^2/(\pi e AR)$.

Added together these form the total drag from constant and α-related influence. The constant part of the formula is

$$C_{D_0} = C_{D_F} S_F/S + C_{D_T}(S_T + S_V)/S + C_{D_E} + C_{d_0}, \tag{26}$$

with the overall formula given by

$$C_D = C_{D_0} + C_{d_L}(C_L - C_{L_{min}})^2 + C_L^2/(\pi e AR). \tag{27}$$

When the side angle β is nonzero, there will also be a side force and additional drag, primarily resulting from the vertical tail acting like a wing, providing "lift" in a sideways direction. Side angle effects are not considered in Beron-Rawdon's paper, so we extrapolate here a roughly approximate formulation. The aspect ratio of the vertical tail is usually much smaller than that of the wing, and here is assumed to be $AR_V = 0.5AR$. From this, the "lift" slope is found similarly to C_{L_α} above, using the same infinite-span wing lift slope a_0 but the new AR_V, and multiplying by the area ratio S_V/S since this sideslip is based on the vertical tail area:

$$C_{C_\beta} = \frac{a_0}{1 + a_0/(\pi e AR_V)} \left(\frac{S_V}{S}\right) \tag{28}$$

(in 1/rad). The tail is symmetrical for stability, so naturally there is no side force when $\beta = 0$, leading to the force equation

$$C_C(\beta) = C_{C_\beta}\beta. \tag{29}$$

The drag resulting from this side angle manifests like the induced drag resulting from a lift force:

$$C_{D_\beta} = C_C^2 \left(\frac{1}{\pi e AR_V}\right)\left(\frac{S}{S_V}\right) \tag{30}$$

(in $1/\text{rad}^2$). The overall aerodynamic force coefficient formulas for use in equations (19-21) are therefore

$$\begin{aligned} C_D(\alpha_w, \beta_w) &= C_{D_0} + C_{d_L}(C_L(\alpha_w) - C_{L_{min}})^2 + (C_L(\alpha_w))^2 \left(\frac{1}{\pi e AR}\right) \\ &\quad + (C_C(\beta_w))^2 \left(\frac{1}{\pi e AR}\right)\left(\frac{S}{S_V}\right) \qquad (31) \\ C_C(\beta_w) &= C_{C_\beta}\beta_w \qquad (32) \\ C_L(\alpha_w) &= C_{L_\alpha}(\alpha_w - \alpha_0). \qquad (33) \end{aligned}$$

The model developed herein is compared with that of [1] in Table 1. This table displays several typical gliding performance benchmarks for wings-level, trimmed, non-accelerating flight, both for this model and that of Beron-Rawdon's study, for a selected set of vehicle parameter combinations $\{\ell, AR, W\}$ reported in [1]. The performance benchmarks are maximum lift/drag ratio $(L/D)_{\max}$, and minimum sink rate $(-\dot{h})_{\min}$. The table also provides the speed V for these flight conditions with the specified parameters, and V for the case where the vehicle sink rate is $2(-\dot{h})_{\min}$. Note that the values of $(-\dot{h})_{\min}$ in the results from [1] remain the same for each $\{\ell, AR\}$ combination. This is because, in that study, W was chosen to result in those specific values. As can be seen from the table, there is good general agreement between our values and those from [1]. The principal qualitative divergence is that our values of $(L/D)_{\max}$ do not vary with W, while those from [1] do, due to the latter study including Reynolds number effects which were ignored in this study. On the other hand, this model provides all necessary aerodynamic parameters for point-mass flight dynamics as continuous functions of the vehicle parameters, while retaining sufficient agreement with data from [1] and [8] to confidently use the model for exploration of small-glider flight dynamics and performance.

In using these models, it must be stressed that the linear and quadratic angle dependencies in the force formulas are approximations which are accurate for small angles; in reality the lift will not actually increase unboundedly as α_w does, for example. Thus, trajectories for this model which involve extreme values of α_w and β_w will be suspect, but for reasonably small values of the control angles these formulas should be accurate enough and appropriate to use. This is especially relevant in the case of smaller, slower gliders, since the aircraft velocity may be on the same order of magnitude as that of the arbitrary ambient wind field through which it flies, with the result that the wind-relative α_w and β_w values that the aircraft may transiently experience could be well outside the range of validity of the quadratic drag/linear lift/linear side force model representation.

Section 6: Glider Model Test Simulations

To test out the glider model equations of motion and the Fortran codes implementing them, we have performed simulations for some simple example problems using the codes. These were done to observe the behavior of the model qualitatively and see how it matches expected behavior for the glider.

Table 1: Comparison of the Current Model Flight Condition Values with Beron-Rawdon Results, over a Range of Glider Configurations.

$\{\ell(\text{in}), AR, W(\text{lb})\}$	$(L/D)_{\max}$	V at $(L/D)_{\max}$	$(-\dot{h})_{\min}$	V at $(-\dot{h})_{\min}$	V at $2(-\dot{h})_{\min}$
$\{60, 6, 0.74\}$	16.3	17.6	1.00	15.0	24.3
B-R Values $\rightarrow$	14.5	16.6	1.00	13.8	24.0
$\{60, 6, 1.78\}$	16.3	27.4	1.55	23.2	37.6
B-R Values $\rightarrow$	16.2	27.7	1.50	20.8	38.8
$\{60, 12, 0.65\}$	21.3	21.7	0.95	18.8	29.6
B-R Values $\rightarrow$	18.3	18.3	1.00	18.3	26.2
$\{60, 12, 1.72\}$	21.3	35.3	1.54	30.5	48.1
B-R Values $\rightarrow$	20.0	32.2	1.50	29.8	46.2
$\{60, 16, 0.50\}$	22.9	21.4	0.87	18.6	29.0
B-R Values $\rightarrow$	18.6	18.6	1.00	18.6	25.9
$\{60, 16, 1.55\}$	22.9	37.6	1.54	32.7	51.1
B-R Values $\rightarrow$	21.8	32.8	1.50	32.8	47.3
$\{100, 6, 2.21\}$	16.3	18.3	1.03	15.6	25.2
B-R Values $\rightarrow$	16.4	18.5	1.00	13.9	26.1
$\{100, 6, 5.29\}$	16.3	28.3	1.60	24.1	38.9
B-R Values $\rightarrow$	17.5	32.2	1.50	22.1	40.2
$\{100, 12, 2.25\}$	21.5	24.3	1.05	21.0	33.1
B-R Values $\rightarrow$	21.2	22.2	1.00	19.8	32.4
$\{100, 12, 5.53\}$	21.5	38.0	1.65	33.0	51.9
B-R Values $\rightarrow$	21.9	36.3	1.50	30.6	52.5
$\{100, 16, 1.97\}$	23.1	25.5	1.03	22.2	34.7
B-R Values $\rightarrow$	22.1	22.1	1.00	22.1	32.6
$\{100, 16, 5.20\}$	23.1	41.4	1.67	36.1	56.4
B-R Values $\rightarrow$	23.5	38.8	1.50	34.6	55.2
$\{140, 6, 4.54\}$	16.4	18.8	1.06	15.9	26.0
B-R Values $\rightarrow$	17.2	20.5	1.00	14.6	26.7
$\{140, 6, 10.9\}$	16.4	29.1	1.64	24.7	40.0
B-R Values $\rightarrow$	18.0	31.8	1.50	23.9	41.0
$\{140, 12, 4.82\}$	21.6	25.4	1.10	22.0	34.6
B-R Values $\rightarrow$	21.8	24.2	1.00	20.6	34.9
$\{140, 12, 11.7\}$	21.6	39.6	1.71	34.3	54.0
B-R Values $\rightarrow$	23.3	39.0	1.50	32.9	55.4
$\{140, 16, 4.57\}$	23.3	27.8	1.11	24.2	37.8
B-R Values $\rightarrow$	23.6	26.0	1.00	23.2	36.7
$\{140, 16, 10.7\}$	23.3	42.6	1.71	37.1	57.8
B-R Values $\rightarrow$	24.8	41.7	1.50	35.1	58.9

A series of simulations were performed which calculated trajectories for gliders given constant control angle inputs at various conditions. The glider used for these simulations had values of $\ell = 60$ in, $AR = 16$, and $W = 3$ lb. The glider was given constant velocity-relative control angles of $\alpha = 10°$, $\beta = 10°$, and $\sigma = -10°$, and initial values of altitude $h = 200$ ft, velocity $V = 47.9$ ft/s, elevation angle $\gamma = -3.32°$, and azimuth angle $\chi = 0°$. In the absence of ambient wind these conditions produce a quasi-steady-state solution, with the glider spiraling downward around a cylinder of constant diameter of about 800 ft, with V and γ remaining constant. The trajectory is shown for 60 seconds of flight in Figure 1 (in two dimensions, from above) and Figure 2 (in three dimensions).

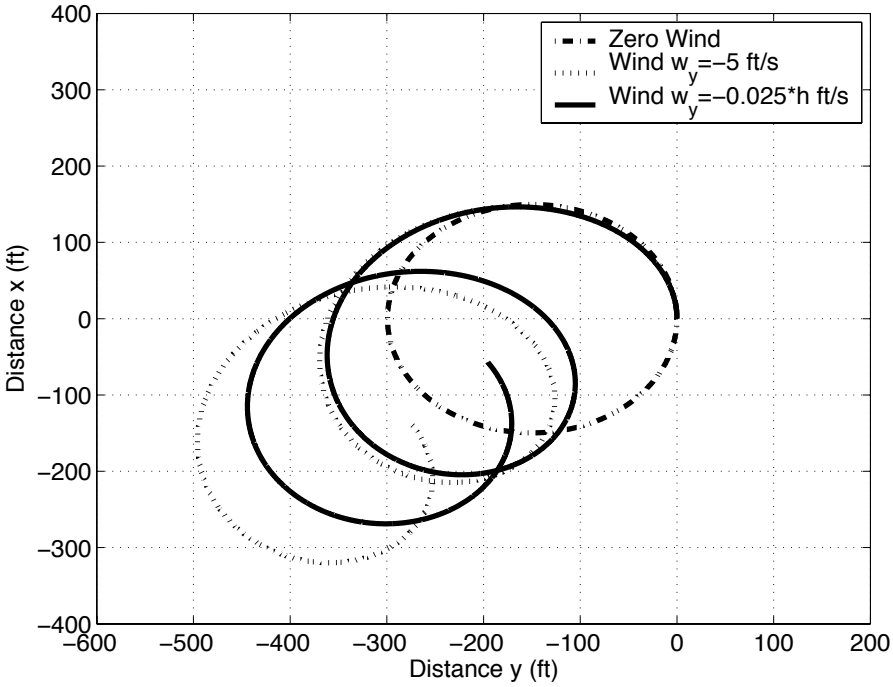

Figure 1: Constant-Control Glider Trajectories – Top View (Configuration 1).

With the addition of a constant-strength $w_y = -5$ ft/s crosswind, the glider drifts off from that cylindrical descent, as the aircraft is aided by the wind during certain portions of the trajectory. This happens specifically when the glider is moving in the negative y direction, with the wind behind it causing it to pick up speed, which then also carries over into the negative x direction part of the trajectory. The glider is slowed down while flying in the positive y direction, impeded by the wind, leaving it slower along the trajectory moving in the positive x direction. In sum this results in a translational motion in the negative y direction being adding to the spiraling path, along with a lesser motion in the negative x direction. The glider also loses slightly more altitude than in the zero-wind case, as the wind makes the glider diverge from the more efficient quasi-steady trajectory.

The third simulation to be performed used a wind gradient of $w_y = -0.025 * h$ ft/s (stronger crosswinds at higher altitudes). At the initial altitude the wind velocity is $w_y = -5$ ft/s, the same as the constant-wind case, and so those two trajectories are similar at first. Then as the

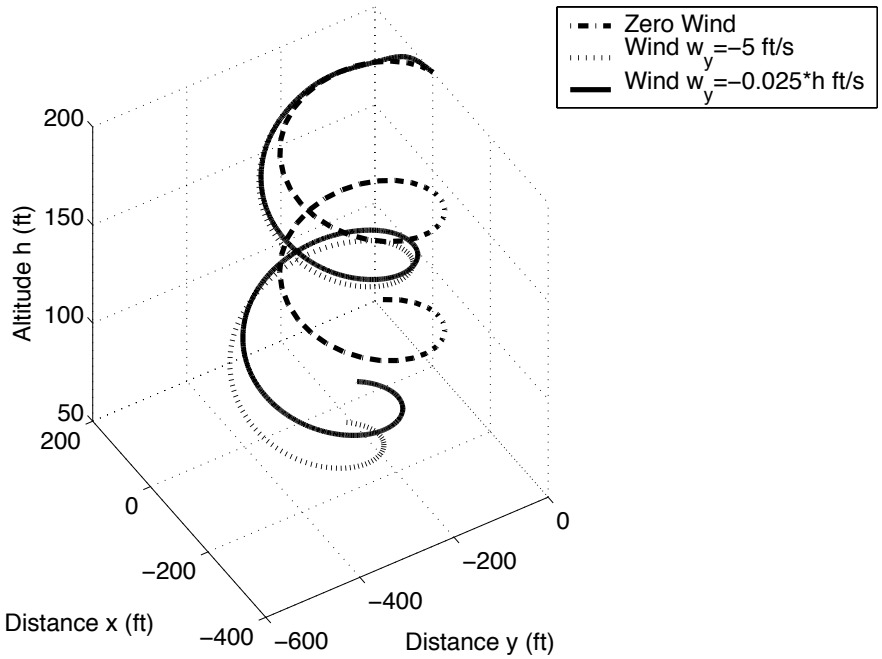

Figure 2: Constant-Control Glider Trajectories (Configuration 1).

glider loses altitude and the wind becomes slower, the trajectory's drift slows and it approaches more of a steady spiral like the zero-wind case. The differences between the three trajectories can be seen in Figures 1 and 2.

The above simulations are also replicated using a different set of glider parameters: $\ell = 100$ in, $AR = 16$, and $W = 4.5$ lb. The larger and heavier glider can catch more passing air and thus gain more force for maneuvering, making it easier for the wind to change the glider's course. As an example of this, with zero wind the second glider configuration has a quasi-steady spiraling path of diameter roughly 100 ft, about one third that of the first glider configuration (of parameters 60/16/3). Although the maximum L/D ratio is almost the same for the two configuration parameter sets, the minimum sink rate is 1.56 ft/s for the second set as compared to 2.14 ft/s for the first. The effect of this can be seen in that the second configuration only loses about 80 ft of altitude during the same sixty seconds of zero-wind descent in which the first configuration loses about 130 ft. In this case the initial conditions for the quasi-steady spiral with velocity-relative control angles $\{\alpha, \beta, \sigma\} = \{10^\circ, 10^\circ, -10^\circ\}$ are altitude $h = 200$ ft, velocity $V = 33.8$ ft/s, elevation angle $\gamma = -3.04^\circ$, and azimuth angle $\chi = 0^\circ$.

Configuration 2 is also used with a constant wind $w_y = -5$ ft/s, and a wind gradient $w_y = -0.025 * h$ ft/s (both as for configuration 1). The three trajectories are plotted in Figure 3 (two dimensions from above) and Figure 4 (three dimensions). As with configuration 1, the spiral predominantly drifts in the negative y direction, and to lesser extent in the negative x direction, as the wind affects the glider's momentum. This is a result, as before, of the changing vehicle orientation with respect to the wind. However, it looks much more extreme here, since there is close to the same amount of drift but reflected on a smaller diameter spiral in the flight path. The wind gradient case also shows, as before, an initially similar path with drift due to

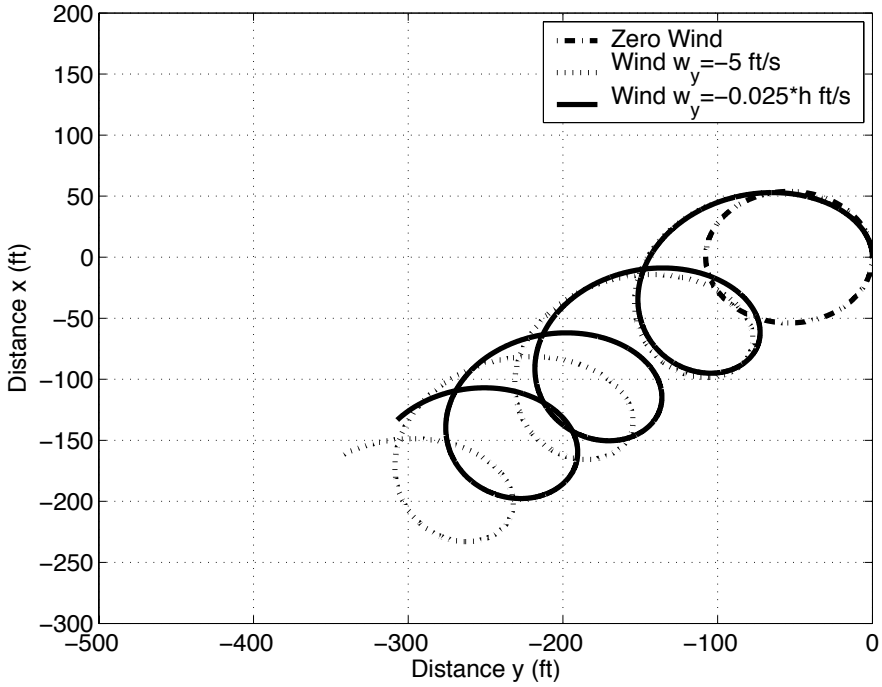

Figure 3: Constant-Control Glider Trajectories – Top View (Configuration 2).

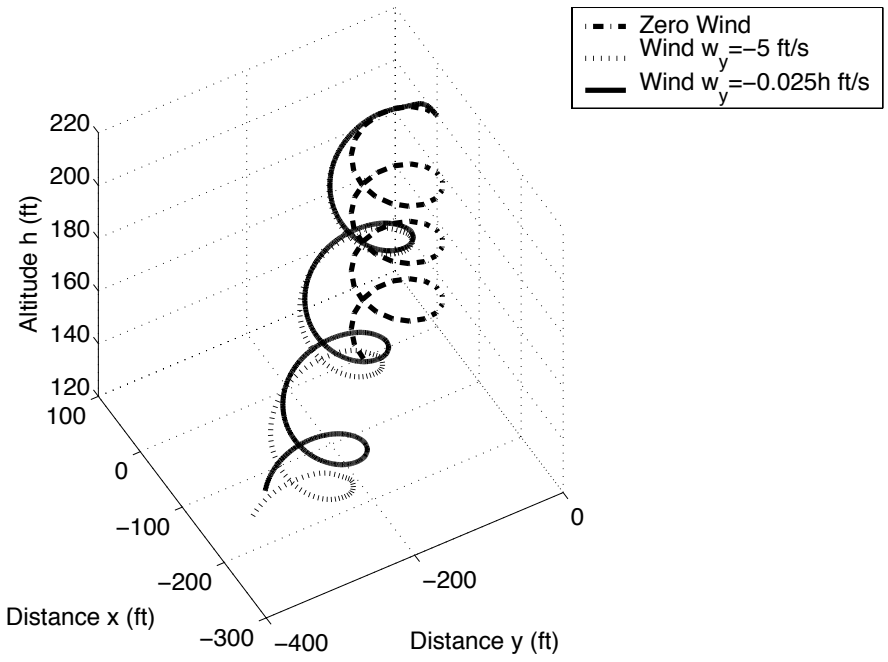

Figure 4: Constant-Control Glider Trajectories (Configuration 2).

the wind, before the drift slows due to the lesser winds at lower altitude.

Figure 5 plots the zero-wind and constant -5 ft/s wind trajectories for both glider configurations, to show the tighter, faster spirals of configuration 2 compared with the slower, larger spiral of configuration 1. As can be seen here, the glider flight behavior varies depending on the

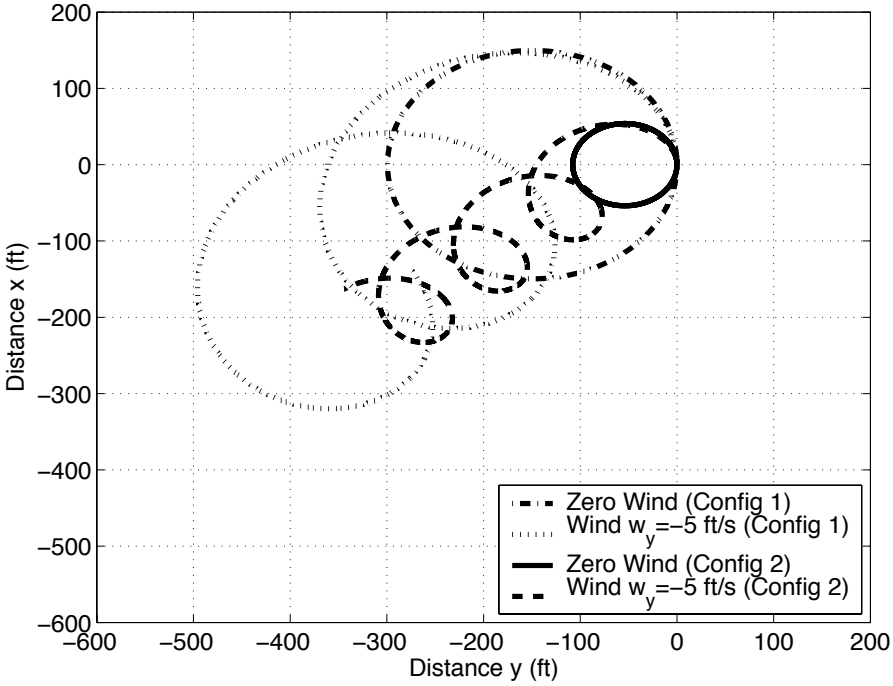

Figure 5: Constant-Control Glider Trajectories – Top View (Both Configurations).

particular glider characteristics and wind strength. Even more extreme differences can result from larger changes in these parameters. For example, greater winds or a lighter, smaller vehicle can result in the glider being completely blown along with the wind, unable even to complete a turn back into the wind with the given control inputs. The particular control inputs used obviously will affect the flight behavior as well. If more extreme control inputs are used, then the wind will strike the aircraft from different angles and the spiral/drift patterns may be greatly altered. For example, a tighter spiral can result in the drift being mostly in the negative x direction, as the accumulated speed has little chance to exert itself before the turn from negative-y to negative-x. A large change in the speed of descent may result as well for changes in the flight conditions.

Section 7: Conclusions

We have presented here a model of glider flight in the presence of ambient winds, which in simulations has resulted in realistic flight properties. The model includes a detailed accounting of the wind effects explicitly in its formulation, not merely as perturbations from a zero-wind base system of equations. Control of the system is achieved through regulation of the velocity-

relative aerodynamic attack, side, and bank angles, which in turn influence the strength and direction of the aerodynamic force vector.

The comparison of $(L/D)_{\max}$, $(-\dot{h})_{\min}$, and $2(-\dot{h})_{\min}$ (and the associated velocities) as calculated by the model described here with their values in [1] results in generally good correspondence. Even where there are differences, a qualitative behavioral match is seen, with the calculated values following similar patterns of change with respect to the parameters $\{\ell, AR, W\}$ as the Beron-Rawdon values do. The test example sets display the flight dynamics behavior of the glider model in different ambient wind conditions and with different physical glider characteristics, looking at the forward solution of the flight dynamics with fixed control input. The generated trajectories show that the model results in believable flight behavior in three dimensions with a range of wind types and for different structural glider characteristics.

With some relatively simple examples having been tested and the simulated glider having reacted in an expected manner, the model is now ready to be used in more complex and useful problems. Three-dimensional trajectory optimization procedures are being studied; in particular we are looking at "dynamic soaring" type behavior, where a maneuverable aircraft can extract energy from a wind gradient and thus minimize its loss of altitude (or even gain altitude) without thrust and in purely horizontal winds. An alternate scenario is flight through a region containing a number of scattered thermal updrafts, with the question of how to optimize the use of such thermals while at the same time following close to a desired flight path. Another avenue of research involves the extension of the model to consider uncertainties in the wind field or other elements, to more realistically represent conditions in the real world. Related to this would be the construction of a feedback control, based on open-loop controls generated using optimization, to allow the glider to respond to unexpected changes or uncertainties in the environment.

Appendix I: Detailed Matrix Rotation Formulation

The Euler rotation sequence $\{\chi, \gamma, \sigma\}$ is expressed by the matrix R_{VI}, and moves from the inertial frame to the velocity frame. The χ rotation about the axis $\hat{z}$ is first, followed by the γ rotation about the y-axis in the new post-χ frame, followed by the σ rotation about the x-axis in the post-χ-post-γ frame. This involves the use of coordinate transformation matrices to ensure that the rotations are done in the correct frame of reference. Therefore, starting from the basic inertial axes $\hat{U}_I$, the χ-rotation matrix R_χ takes these to the post-χ frame axes (in inertial coordinates): $\hat{U}_a = R_\chi \hat{U}_I$. The transformation matrix from these new $\hat{U}_a$ coordinates to inertial coordinates is given by that set of axes ($T_{Ia} = \hat{U}_a$).

Since the next rotation (through γ) is done in the post-χ frame, the T_{Ia} coordinate transformation must be used before and after the rotation, resulting in $\hat{U}_b = (T_{Ia} R_\gamma T_{Ia}^{-1})\hat{U}_a = \hat{U}_a R_\gamma$, and $T_{Ib} = \hat{U}_b$. The σ-rotation similarly must have the T_{Ib} transformation before and after it to change into post-χ-post-γ coordinates and back. This results in $\hat{U}_V = (T_{Ib} R_\sigma T_{Ib}^{-1})\hat{U}_b = \hat{U}_b R_\sigma$. Now, since overall we are in inertial frame coordinates, defined as $\hat{U}_I = I$, this means $\hat{U}_a = R_\chi$ and $\hat{U}_b = \hat{U}_a R_\gamma = R_\chi R_\gamma$. Therefore the final result of the sequence of three rotations in three different reference frames is $R_{VI} = \hat{U}_V = \hat{U}_b R_\sigma = R_\chi R_\gamma R_\sigma$.

This shows that the combined rotation process from the inertial frame axes to the velocity frame axes is equivalent to doing the three individual matrix rotations all about the original

inertial frame axes ($\hat{z}$, $\hat{y}$, and $\hat{x}$), but in the reverse order, as given by:

$$R_{VI} = \begin{bmatrix} \cos\chi & -\sin\chi & 0 \\ \sin\chi & \cos\chi & 0 \\ 0 & 0 & 1 \end{bmatrix} \begin{bmatrix} \cos\gamma & 0 & \sin\gamma \\ 0 & 1 & 0 \\ -\sin\gamma & 0 & \cos\gamma \end{bmatrix} \begin{bmatrix} 1 & 0 & 0 \\ 0 & \cos\sigma & -\sin\sigma \\ 0 & \sin\sigma & \cos\sigma \end{bmatrix}. \tag{34}$$

The rotation R_{BV} through $-\beta$ and α is given by:

$$R_{BV} = \begin{bmatrix} \cos\alpha & 0 & \sin\alpha \\ 0 & 1 & 0 \\ -\sin\alpha & 0 & \cos\alpha \end{bmatrix} \begin{bmatrix} \cos\beta & \sin\beta & 0 \\ -\sin\beta & \cos\beta & 0 \\ 0 & 0 & 1 \end{bmatrix}. \tag{35}$$

This is not an Euler sequence as in equation (34) where the three angles are reversed due to the nature of the rotation sequence. Here both rotations are considered to be about the velocity axes, since they represent comparatively small divergences from those axes in the horizontal and vertical directions, and so they are expressed appropriately in this order.

Similarly to equations (34-35), the sequences of rotations through the wind-relative frame are given by:

$$R_{WI} = \begin{bmatrix} \cos\chi_w & -\sin\chi_w & 0 \\ \sin\chi_w & \cos\chi_w & 0 \\ 0 & 0 & 1 \end{bmatrix} \begin{bmatrix} \cos\gamma_w & 0 & \sin\gamma_w \\ 0 & 1 & 0 \\ -\sin\gamma_w & 0 & \cos\gamma_w \end{bmatrix} \begin{bmatrix} 1 & 0 & 0 \\ 0 & \cos\sigma_w & -\sin\sigma_w \\ 0 & \sin\sigma_w & \cos\sigma_w \end{bmatrix}, \tag{36}$$

$$R_{BW} = \begin{bmatrix} \cos\alpha_w & 0 & \sin\alpha_w \\ 0 & 1 & 0 \\ -\sin\alpha_w & 0 & \cos\alpha_w \end{bmatrix} \begin{bmatrix} \cos\beta_w & \sin\beta_w & 0 \\ -\sin\beta_w & \cos\beta_w & 0 \\ 0 & 0 & 1 \end{bmatrix}. \tag{37}$$

The process of finding the unknown wind-relative angles for evaluating the equations of motion begins with the knowledge that $\hat{x}_w = R_{WI}\hat{x}$, from which we can find χ_w and γ_w. Componentwise this requirement is

$$\hat{x}_w = \begin{bmatrix} \cos\chi_w \cos\gamma_w \\ \sin\chi_w \cos\gamma_w \\ -\sin\gamma_w \end{bmatrix}, \tag{38}$$

with $\hat{x}_w = \vec{V}_w / \|\vec{V}_w\|$. The angles are computed by

$$\gamma_w = \sin^{-1}(-(\hat{x}_w)_3), \tag{39}$$

$$\chi_w = sign((\hat{x}_w)_2 / \cos\gamma_w) \cos^{-1}((\hat{x}_w)_1 / \cos\gamma_w). \tag{40}$$

The value of γ_w found by the inverse sine is unique, due to the restriction $|\gamma_w| \leq \pi/2$, which maintains the uniqueness of the rotational angle sequence. The sign check in equation (40) ensures that the correct inverse cosine solution has been used.

To find the remaining wind-relative angles we use equation (18), which can be slightly rewritten (moving the known χ_w and γ_w terms to the opposite side of the equation) to produce:

$$\begin{aligned} \tilde{M} &\equiv \begin{bmatrix} \cos\gamma_w & 0 & -\sin\gamma_w \\ 0 & 1 & 0 \\ \sin\gamma_w & 0 & \cos\gamma_w \end{bmatrix} \begin{bmatrix} \cos\chi_w & \sin\chi_w & 0 \\ -\sin\chi_w & \cos\chi_w & 0 \\ 0 & 0 & 1 \end{bmatrix} R_{VI} R_{BV} \\ &= \begin{bmatrix} 1 & 0 & 0 \\ 0 & \cos\sigma_w & -\sin\sigma_w \\ 0 & \sin\sigma_w & \cos\sigma_w \end{bmatrix} \begin{bmatrix} \cos\alpha_w & 0 & \sin\alpha_w \\ 0 & 1 & 0 \\ -\sin\alpha_w & 0 & \cos\alpha_w \end{bmatrix} \begin{bmatrix} \cos\beta_w & \sin\beta_w & 0 \\ -\sin\beta_w & \cos\beta_w & 0 \\ 0 & 0 & 1 \end{bmatrix}. \end{aligned} \tag{41}$$

The third column of this matrix equality is given by

$$\tilde{M}_{(1..3,3)} = \begin{bmatrix} \sin\alpha_w \\ -\sin\sigma_w \cos\alpha_w \\ \cos\sigma_w \cos\alpha_w \end{bmatrix}. \tag{42}$$

Thus we can calculate α_w and σ_w by:

$$\alpha_w = \sin^{-1}(\tilde{M}_{(1,3)}), \tag{43}$$

$$\sigma_w = sign(-\tilde{M}_{(2,3)}/\cos\alpha_w)\cos^{-1}(\tilde{M}_{(3,3)}/\cos\alpha_w). \tag{44}$$

As with equation (39), the value of α_w in equation (43) is found uniquely by the inverse sine function since $|\alpha_w| \leq \pi/2$. Also, as in equation (40), the sign check in equation (44) serves to specify the correct inverse cosine solution for σ_w. The angle β_w is found in a similar manner, starting with the first row of the matrix equality in equation (41):

$$\tilde{M}_{(1,1..3)} = \begin{bmatrix} \cos\alpha_w \cos\beta_w & \cos\alpha_w \sin\beta_w & \sin\alpha_w \end{bmatrix}, \tag{45}$$

and evaluating the equation

$$\beta_w = sign(\tilde{M}_{(1,2)}/\cos\alpha_w)\cos^{-1}(\tilde{M}_{(1,1)}/\cos\alpha_w). \tag{46}$$

With the values for all of the wind-relative angles found, the aerodynamic force terms can be found using equations (19-23).

References

[1] Beron-Rawdon, B., "Performance Analysis of a Family of R/C Thermal Sailplanes," R/C Soaring UK, http://www.rc-soar.com/tech/perfanal.htm (2000).

[2] Etkin, B., *Dynamics of Atmospheric Flight*, New York, New York: John Wiley and Sons, 1972.

[3] Sachs, G., Knoll, A., and Lesch, K., "Optimal Utilization of Wind Energy for Dynamic Soaring," Technical Soaring, Vol. 15, No. 2, pp. 48-55 (1991).

[4] Sachs, G., "Optimal Wind Energy Extraction for Dynamic Soaring," in *Applied Mathematics in Aerospace Science and Engineering*, edited by Miele, A. and Salvetti, A., pp. 221-237, New York, New York: Plenum Press, 1994.

[5] Goto, N. and Kawable, H., "Direct Optimization Methods Applied to a Nonlinear Optimal Control Problem," Mathematics and Computers in Simulation, Vol. 51, pp. 557-577 (2000).

[6] Perkins, C. D. and Hage, R. E., *Airplane Performance Stability and Control*, New York, New York: John Wiley and Sons, 1949.

[7] Anderson, J. D., *Introduction to Flight* (Fourth Edition), Boston, Massachusetts: McGraw-Hill, 2000.

[8] Selig, M. S., Donovan, J. F., and Frasier, D. B., *Airfoils at Low Speeds*, Soartech 8, Virginia Beach, Virginia: H. A. Stokely, 1989.

REPORT DOCUMENTATION PAGE	Form Approved OMB No. 0704–0188

1. REPORT DATE *(DD-MM-YYYY)*	2. REPORT TYPE	3. DATES COVERED *(From - To)*
01-11-2003	Technical Memorandum	

4. TITLE AND SUBTITLE
A Flight Dynamics Model for a Small Glider in Ambient Winds

5a. CONTRACT NUMBER

5b. GRANT NUMBER

5c. PROGRAM ELEMENT NUMBER

6. AUTHOR(S)
Scott C. Beeler, Daniel D. Moerder, and David E. Cox

5d. PROJECT NUMBER

5e. TASK NUMBER

5f. WORK UNIT NUMBER
23-762-40-41

7. PERFORMING ORGANIZATION NAME(S) AND ADDRESS(ES)
NASA Langley Research Center
Hampton, VA 23681-2199

National Institute of Aerospace (NIA)
144 Research Drive
Hampton, VA 23666

8. PERFORMING ORGANIZATION REPORT NUMBER
L–18338

9. SPONSORING/MONITORING AGENCY NAME(S) AND ADDRESS(ES)
National Aeronautics and Space Administration
Washington, DC 20546-0001

10. SPONSOR/MONITOR'S ACRONYM(S)
NASA

11. SPONSOR/MONITOR'S REPORT NUMBER(S)
NASA/TM–2003–212665

12. DISTRIBUTION/AVAILABILITY STATEMENT
Unclassified-Unlimited
Subject Category 02
Availability: NASA CASI (301) 621-0390 Distribution: Standard

13. SUPPLEMENTARY NOTES
Beeler, National Institute of Aerospace. Moerder and Cox, NASA Langley Research Center.
An electronic version can be found at http://techreports.larc.nasa.gov/ltrs/ or http://ntrs.nasa.gov/

14. ABSTRACT

In this paper we describe the equations of motion developed for a point-mass zero-thrust (gliding) aircraft model operating in an environment of spatially varying atmospheric winds. The wind effects are included as an integral part of the flight dynamics equations, and the model is controlled through the three aerodynamic control angles. Formulas for the aerodynamic coefficients for this model are constructed to include the effects of several different aspects contributing to the aerodynamic performance of the vehicle. Characteristic parameter values of the model are compared with those found in a different set of small glider simulations. We execute a set of example problems which solve the glider dynamics equations to find the aircraft trajectory given specified control inputs. The ambient wind conditions and glider characteristics are varied to compare the simulation results under these different circumstances.

15. SUBJECT TERMS
Glider aerodynamics, Soaring aircraft, Mathematical models of aircraft, Low speed aerodynamics, Aerodynamic coefficients

16. SECURITY CLASSIFICATION OF:			17. LIMITATION OF ABSTRACT	18. NUMBER OF PAGES	19a. NAME OF RESPONSIBLE PERSON
a. REPORT	b. ABSTRACT	c. THIS PAGE			STI Help Desk (email: help@sti.nasa.gov)
U	U	U	UU	20	19b. TELEPHONE NUMBER *(Include area code)* (301) 621-0390